Impact of Pollutants in Surface Water Ecosystem using Hybrid Stochastic Geometry

UDAYAKUMAR ALLIMUTHU*, C. EDWIN SINGH, SARAVANAN MATHESWARAN
Department of Computer Science and Engineering , School of Computing,
Vel Tech Rangarajan Dr. Sagunthala R&D Institute of Science and Technology,
Avadi, Chennai, Tamilnadu,
INDIA

**Corresponding Author*

Abstract: - The structural and ecological functions and the physical environment factor for the surroundings are used to compare the interrelated components to manage the boundaries and the terrestrial aspect of the aquatic systems. The problem of freshwater contamination can be evaluated to produce the marine ecosystem, and the marine ecosystem can be elaborated. By changing the chemical and biological characteristics, the water purity and the components of the water can be evaluated. The materials used in the research are MnWO4 / g-C3N4**,** BiVO4 / g-C3N4, ZnWO4 / g-C3N4, and CuWO4 / g-C3N4 used to obtain the 4-chlorophenol (4-CP), and Rhodamine B (RhB) by using the Photocatalytic Mechanism, the method of Hybrid Stochastic geometry. It consists of an Enhanced Reaction and Diffusion mathematical statement that can be proposed for dissolving oxygen using the Combined Phase Space Method equations. This study focused on modeling a time series on a suspension matter using the Bayesian Structural Time Series technique (BSTS). The statistical results were based on simulation procedures that employed the Kalman filter and the Monte Carlo Markov Chain (MCMC). The nutrients that tend to the 0 contractions in the study produce the eutrophication of the incorporating that can be managed in the population, and the recycling of the Photocatalytic chemicals was evaluated. Maintaining the standard model for the pollution on the surface of the water and modeling the ecosystem can be done to elaborate the surface of the water mode.

Key-Words: - Ecology Functions, Marine Ecosystem, Biological Water Purity, Photocatalytic, Stochastic Geometry, Phase Space Method, Time Series Technique.

Received: June 29, 2024. Revised: January 9, 2025. Accepted: February 24, 2025. Published: March 26, 2025.

1 Introduction

In the world, clean water is at high risk. The pollution of the coastal areas and seas poses. The aquatic ecosystem makes the representative and the society which enables the mathematical models and the continental scale, which allows the multi-pollutant modeling and the multiple impacts of the various types of the new generations of the integration of the water and the pollutions which enables the exposure and the integration of the water quality and the assessment of the quality issues. The aquatic ecosystem manages the new generations, and the multiple impacts of the quality issues will maintain the explicit factor for the pollutant factorization of the coastal areas can be done in the aquatic ecosystem. Also, the process of multiple pollutants and the combination of the exposure and the issues in the water quality can happen in the global continental model for the quality assessments. To focus on the quality of the services and the water quantity, which enables the sustainable factor for the development of the goals and the threat of the water quantity can be evaluated based on the hypoxia for human health. The water surfaces can be elaborated during the multiple impacts of the pollutants. Human activities enable the use of plastic chemicals, and the management of the contaminants and the needs and nutrients of the open defecation for the water's surface can be evaluated. So, the primary source of agriculture can be assessed by the recovery and the regional differences, which enables the cause of the surface water and the excretion of the water in the environmental factorization, which elaborates the continental analysis. In this novel, the decision, which is based on the exercises and the pollutants of the water, can be evaluated for the multiple contaminants and the abovementioned pollutant, which enables the first modeling of the biological factor of the water to be considered for the

environmental factors can be done in the regions. The modeling of the water pollutants can be evaluated, [1]. The comprehensive and integrated factors for the multi pollutants and the pathogens that enable the antibodies and changes in the river temperature, which enables the nutrients and the pathogens of the nanomaterials for several reasons, can be evaluated for the model of multi pollutants. The pollution made by the environment and humans can be assessed, which makes the particular factor for the river temperature and the exact address which manages the nanomaterials and the completion of the quality in the variables, and the water pollution surfaces can be evaluated for the nutrients, [2]. The pathogens and the flow of the climatic changes can be assessed. The ecosystem, types of ecosystem, and the surface structure of the environmental pollution can be evaluated for the harmful biotic components and the pollutants that enable the environmental carbon monoxide to produce sulfur and gaseous pollution in the water.
The contribution of this study is as follows:

1. The proliferation of pollutants in the surface water ecosystem may be assessed and resolved by using mathematical modelling that captures the essence of the impacts of pollution depending on favourable conditions.
2. The Stochastic geometry, Reaction and Diffusion, Phase Space Method, and Time Series technique model can be evaluated to enable the reduction of Pollutants in the Surface Water Ecosystem, which will produce stability in the environment and reduce pollution.

2 Literature Review

The surface water in the countries of Asia, which focuses on the pollution of risk, and the perspectives of the risks in the future can be evaluated, [3]. Also, the water in East Asia can be detected with more antibodies, and this is the review in the water, as well as the aquaculture, and the urban area evolves the surface of the water. The water humidity can be evaluated in urban areas. Also, the regional monitoring of the environmental guidelines for the antibodies is a need in this study is proposed. Also, by implementing this in the currently proposed system, regional tracking can be done in the future.

According to the ecological and health risk evaluation research, the 10 trace elements in surface water may be used to assess the ecological and health risk factors for fish breeding in terms of the noncarcinogenic risk, [4]. The trace elements for analyzing the metal toxicity can be elaborated. Also, the process of carcinogenic risk for the adults and children who enable the properties and the dry season which produces the collection of the metal society can be elaborated. By involving this in the currently proposed system, the water sample can also be evaluated in the culture.

Implementing emerging pollutants and endocrine disruptors system, the sensitive online solid phase extraction, and the development of the assessing occurrence mange's biological significance can be evaluated. The groundwater flow for the relevance and the regulatory nutrients for encouraging the municipal factorization and the population areas can be assessed for the water ecosystem. The distribution of endocrine and pharmaceuticals and the production of aquatic and municipal wastewater factorization can be elaborated using the contaminations and the rich collection of municipal care products to encourage South Florida, [5].

Identify and manage the procedure of surface water contamination Expanding businesses may promote highly speculative pollution, according to a research by treatment methods for wastewater, the microorganisms can help identify the origins of the most prevalent wastewater discharges [6]. The understanding of the treatment methods for wastewater can be elaborated. Maintaining harmful pollutants and the most common water quality discharge can be analyzed using stemming pollution. By implementing this in the currently proposed system, the wastewater can be evaluated using the suspectable factorization in human activities.

In Environmental regulation, pollution reduction and green innovation research discussed about how environmental management of pollution and green innovation contribute to China's ecological civilization by reducing urban and water pollution emissions. These environmental parameters for pollutant emission in Chinese water were implemented using the population-based analytical framework, [7]. The significant regional population for the water environmental civilization and the difference in the integration of the natural experiments and the pollution index enables the result that shows the regional difference model for the unified analytical factorization to be evaluated. And the policy of the WECCP regional solution can be assessed.

The water quality assessment research examined the complicated indicators of water quality and the southern surface water of the Bug River basin, [8]. The process of managing the water quality

assessment and the southern river bug for finding the basin in the regions is identified by the potential and the capability of the needs and the environmental risks for enveloping the operations and the increase in the urination and the water quality is produced for the southern bug river. The water is tested for the surface river system to make recommendations for the environments and the cultural and statistical factors that envelop the energy complexes. The surface water quality under the complex indices is done by implementing this in the currently proposed system.

3 Proposed Four Photocatalytic System

Industrial (waste)water contains hazards that induce danger to the environment. Numerous dyes are used in industrial, textile, and various business sectors. Various advanced evocation kinds of research are created, like coagulation, adsorption, extraction, and chemical oxidation process, and visible-light photocatalysts as a stable and efficient method for toxic pollutant degradation, [9]. This research synthesized hybrid heterojunction photocatalysts of various nanomaterials such as $MnWO_4$, $CuWO_4$, and $ZnWO_4$. Graphitic carbon nitride is a semiconductor material that improves the charge partition efficiency under visible light owing to energy gap, high thermal, and stability. Each nanoparticle is degraded with tungstate nanorods via the facile hydrothermal method. The Bayesian Structural Time Series technique was used for all photocatalysts to determine the time rate of pollutants' degradation. The resulting heterostructure shows excellent performance in degrading toxic, stable pollutants such as rhodamine B (RhB) and para-chlorophenol (4-CP). Because of the heterojunction photocatalyst simple preparation method and excellent photocatalytic performance, it has great potential for addressing environmental issues. **Materials and Methods:** All the chemicals are used directly with purity. The materials used in the below research are sodium tungstate, manganese sulfate, Zinc nitride, Bismuth nitrate pentahydrate, and venadylacetonate, which are chemicals used to obtain the 4-chlorophenol (4-CP) and Rhodamine B (RhB) dyes, [10].

3.1 Synthesis of MnWO4 / g-C3N4 Nanomaterial

The nanoparticles/nanocomposites are prepared by using the facile hydrothermal route method. Initially, the manganese sulfate and sodium tungstate are taken with a ratio of 1:2 that is reduced to a liquid form by adding 50 ml of deionized water with the help of a 100 ml beaker. This matter was heated to gain a homogeneous mixture and maintained at 120oC for 24 hours in a Teflon-line autoclave. Bare g-C3N4 was synthesized from the annealing for 2 hours at 400oC in an environment. To disseminate g-C3N4, graphitic carbon nitride was Putin to the methanol and ultrasonically stirred for 1 hour. Then MnWO4 was successfully mixed into a solution, stirred for 24 hours, dried at 100oC overnight, and then heated to 300^{o}C for 2 hours. Finally, the nanomaterial has a different ratio of g-C3N4 to MnWO4. The weighted ratio of the materials is 1:1, 2:1, and 3:1. These material samples are labeled GMW1, GMW2, and GMW3, [11].

3.1.1 Photocatalytic Setup

The visible-light photocatalysts are a stable and efficient method for degrading toxic pollutants such as 4-chlorophenol (4-CP) and Rhodamine B (RhB). Here, we use a light source, XQ-500W, with an intensity of 40mW/cm^2 of Xenon lamp that aims to activate the irradiation process in photocatalytic. An experiment setup is covered with a photo-reactor of 500ml capacity with 20×15cm height and dimension. The below procedure is repeated for every two dyes, [12]. At first, the 10 mg catalyst powder was mixed with 50 ml dyes, stirring for 30 minutes to achieve the adsorption-desorption equality. Then, the UV- vis NIR spectrometer observed the ability of 4-chlorophenol (4-CP) and Rhodamine B (RhB) absorption at a bandwidth of 220nm and 540nm, respectively. The activation time of the time source varied from 0- 100 min, with the optimum interval being 20 minutes. The photocatalysis mechanism only satisfies three conditions: first, a light source with significant bandwidth; second, a catalyst (MnTiO2); and finally, oxygen. Homogeneous occurs when both the reactant and catalyst exist in the same phase. The 20 mg L^{-1} dye with photocatalyst is first taken and irradiated under the vis at various times. The RhB degradation efficiency of the catalyst bare g-C_3N_4 and MnWO4 is 32% and 38 %. The degradation efficiency of g-C_3N_4 is increased slowly when MnWO4 is added. The chemical oxygen demand (COD)and total efficiency carbon efficiency (TOE) methods assess the high catalytic nature of the catalyst, [13]. The GMW3 demonstrates that RhB has a high-rate constant of 0.0923 min^{-1}, four times higher than the MnWO4 catalyst 0.0231 min^{-1}.

$$\text{Elimination of COD (\%)} = \frac{OD_I - OD_F}{OD_I} * 100 \quad (1)$$

$$\text{Elimination of TOE (\%)} = \frac{CE_I - CE_F}{CE_I} * 100 \quad (2)$$

where, where: OD_I , OD_F refers to the starting and ending COD in (mg/L) respectively, CE_I denotes starting carbon efficiency and CE_F The experimental wastewater analyses were replicated for each dye as final carbon efficiency. When the COD was tracked together with its run, then this allows the kinetic process and its first order model to be expressed as follows:

$$F_r = \frac{dR}{dt} = -kR \quad (3)$$

Fr denotes the reaction rate with a const of k for the (R)COD residuals concertation at t time. The integration of the above equations is conveyed as follows:

$$R(t) = R_0 \exp(-kt) \quad (4)$$

The half-life time is determined merely as a reaction rate constant by using a pseudo-first-order model, and it is expressed as:

$$t_{1/2} = \ln 2/k = 0.693/k \quad (5)$$

From this analysis, the GMW3 catalysts obtained the highest decolorization efficiency, 91%, and 87%, for the COD elimination efficiency of RhB and 4-CP toxic pollutants.

3.1.2 Photocatalytic Mechanism of MnWO4

When WO4 photocatalysts are present, the photocatalytic reaction is a free radical reaction brought on by light exposure. The photocatalyst surface gets activated and electrons move from the Conduction band (CB) to the Valance band (VB) when the energy of light radiation approaches or surpasses the bandgap of WO4, [14]. The formation of electron-hole pairs in the VB coincides with the formation of electron holes in the CB. Because CB holes lose electrons and function as reducing agents, they exhibit a high oxidation reaction activity (1.0~3.5V) and excellent reducibility (0.5~1.5 V) when reduced. When exposed to light, WO4's VB (hv_{VB}^{+}) and CB (E_{CB}^{-}) and CB (E_{CB}^{-}) produce positive holes and electrons. CB holes have high oxidation reaction activity (1.0~3.5V) because they lose electrons and act as reducing agents and E_{CB}^{-}Ve good reducibility (0.5~1.5 V) when reduced. Positive holes and electrons are generated in the VB (hv_{VB}^{+}) and CB (E_{CB}^{-}) Of WO_4 when exposed to light.

$$hv + WO_4 \rightarrow hv_{VB}^{+} + E_{CB}^{-} \quad (6)$$

$$OH_S^{-} + hv_{VB}^{+} \rightarrow OH^{\bullet} \quad (7)$$

$$H_2O^{abs} + hv_{VB}^{+} \rightarrow OH^{\bullet} + h^{+} \quad (8)$$

$$O^{abs} + E_{CB}^{-} \rightarrow OH_2^{-\bullet} \quad (9)$$

$$Org + hv_{VB}^{+} \rightarrow P_{OXIDATION} \quad (10)$$

The holes in the valance band can be either hydroxyl radicals or directly react with the organic molecules and oxidise subsequently, [15]. The reaction between electrons and organic chemicals produces the reduction product. Photogenerated electrons react with oxygen, [16].

$$Dye + hv_{VB}^{+} \rightarrow P_{OXIDATION} \quad (11)$$

$$Dye + OH^{\bullet} \rightarrow P_{DEGRADATION} \rightarrow CO_2 + H_2O \quad (12)$$

$$Dye + E_{CB}^{-} \rightarrow P_{REDUCTION} \quad (13)$$

Consequently, it is reduced to a superoxide radical anion, which then combines with photons to generate peroxide radicals, [17].

$$H_2O + hv_{VB}^{+} \rightarrow HO^{\bullet} + H^{+} \quad (14)$$

$$hv_{VB}^{+} + OH^{-} \rightarrow HO^{\bullet} \quad (15)$$

$$E_{CB}^{-} + O_2 \rightarrow O_2^{\bullet -} \quad (16)$$

$$O_2^{\bullet -} + H^{+} \rightarrow HO_2^{\bullet} \quad (17)$$

The WO_4 is modified because of the light irradiation and the metal ions when the electrons are excited, and that has significant energy for light absorption and the WO_4 surface to transmit electrons, [18]. It stimulates more electrons in the presence of light, which advances the redox reactions, [19]. On the other hand, the dye molecule's direct absorption of light may enhance electron transfer from the conduction band to the valance band, which is stated as follows:

$$D_{ad} + hv_{VB}^{+} \rightarrow D_{ad}^{*} \quad (18)$$

$$D_{ad}^{*} + WO_4 \rightarrow D_{ad}^{+\bullet} + WO_4(e_{CB}^{-}) \quad (19)$$

The photocatalyst for various dyes was also investigated using the above method, [20].

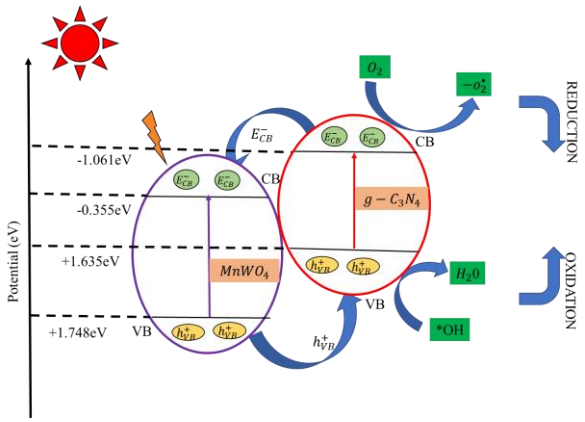

Fig. 1: Proposed mechanism of photocatalytic in g-C3N4/ MnWO4 nanomaterial

3.2 Synthesis of BiVO4 / g-C3N4 Nanomaterial

The bismuth vanadate ($BiVO_4$) acts as a photocatalyst, vis-light driven, and highly responsive owing to its 2.4eV bandgap energy, [21]. This study presents the $BiVO_4$ with different semiconductor g-C3N4 pair weighted ratios. We used a one-step easy hydrothermal approach technique to create the BiVO4 nanoparticles. Initially, we dissolved 0.5g of venadylacetonate (C_{10}, H_{14}, O_5V) in 50mL of deionized water after dispersing 1.2g of Bi $(NO_3)_3.2H_2O$ (Bismuth nitrate pentahydrate). For half an hour, this mixture was agitated, [22]. After finishing the stirring, the NaOH was added to maintain a pH of 8; then, the dispersion was placed in a Teflon-lined stainless-steel reaction vessel and heated to 150°C for 12 hours, then cooling intuitively. The synthesised sample is annealed at 300°C for 4 hours for sample nature. The g-C_3N_4 is added to methanol and ultrasonically stirred for one hour to disperse it. After that, the solution is dried, and power is obtained. These samples are labeled GBV1, GBV2, and GBV3, [23].

3.2.1 Photocatalytic Setup

The visible light under photocatalysts is a stable and efficient method for degrading toxic pollutants such as 4-chlorophenol (4-CP) and Rhodamine B (RhB). The light source from the MnWO4 is used. The 30-minute stirring of the resultant suspension remains unchanged, and the concentration possessed by the dark absorption equilibrium is earlier than the visible irradiation, [24]. Under the vis illumination, the removal efficiency of 29% and 37% attained by the RhB and 4-CP has, respectively, for the Bare $BiVO_4$. When the $BiVO_4$ is loaded into the g-C_3N_4, a significant improvement is monitored in the photodegradation efficiency.

For the RhB and 4-CP, the GBV3 catalyst achieved a final degrading efficiency of 95% and 89%, respectively, [25]. The elimination of harmful contaminants as well as the catalyst's photocatalytic degradation capability are examined using the first-order kinetic relation. It is said as follows:

$$r = \frac{dCons}{dT} = D_{app} * Cons \quad (20)$$

$$\ln\frac{Cons_o}{Cons_T} = D_{app} * T \quad (21)$$

where r denotes degradation rate ($mg.I^{-1}.min^{-1}$), D_{app} refers to apparent degradation constant (min^{-1}), $Cons$ (mg/l) refers to concertation at T(min) irradiation time. The C_{app} is 0.0821 min^{-1} and 0.0563 min^{-1} for RhB and 4-CP, 3.5 times and 2. 7 times more efficient than the bare minimum $BiVO_4$. The third GBV3 catalyst ratio of BiVO4 / g-C3N4 shows better degradation efficiency. Furthermore, the 4:1 and 5:1 ratios of catalysts of BiVO4 / g-C3N4 are labeled as GBV4 and GBV5, respectively—the degradation efficiency of GBV1, GBV2, and GBV3. GBV4 and GBV5 are 41%, 77%,89%,81%, and 71%, respectively, [26]. As a result, the third catalyst shows a superior degradation efficiency compared to the other catalysts

3.2.2 Photocatalytic Mechanism of BiVO4

The degradation mechanism depends on the valence band (VB) at the top and the conduction band (CB) at the bottom of BiVO4 / g-C_3N_4 nanomaterial, calculated by using.

$$E_{CB}^{-} = E_{VB}^{-} + E_{eg}^{-} \quad (22)$$

where, E_{eg}^{-} It is the semiconductor's band gap energy. From Figure 1, the estimated Conduction band and VB of BiVO4 material are 0.042eV and 1.62 eV; for g-C_3N_4, they are 0.034eV and 1.72eV, respectively, [27].

In BiVO4, electrons are transported to the conduction band (CB) holes by photogenerated electron-hole pairs when exposed to visible light with enough excitation energy, [28]. Excited electrons in BiVO4 CB may move to VB and reduce O2 to form superoxide radical (O2•) and hydroxyl radical (OH•), which destroy dye molecules, [29]. The degradation could be significantly influenced by dye absorption on the g-C3N4 surface and electron-hole pairs.

$$E_{CB}^{-} + \text{Dye} \rightarrow Dye^{-\bullet} \quad (23)$$

$$h_{VB}^{+} + \text{Dye} \leftarrow Dye^{+\bullet} \quad (24)$$

$$E_{CB}^{-} + O_{2(aq)} \rightarrow O_2^{\bullet} \quad (25)$$

$$E_{CB}^{-} + O_{2(aq)} + H^{+} \rightarrow HO_2^{\bullet} \quad (26)$$

$$h_{VB}^{+} + OH^{-} \leftarrow OH^{\bullet} \quad (27)$$

$$h_{VB}^{+} + HO_2 \rightarrow H^{+} + OH^{\bullet} \quad (28)$$

In the meantime, the adsorbed OH (hydroxyl)ion on the surface is reduced using the holes in VB of BiVO4's that produce OH•, which can react with target products, [30].

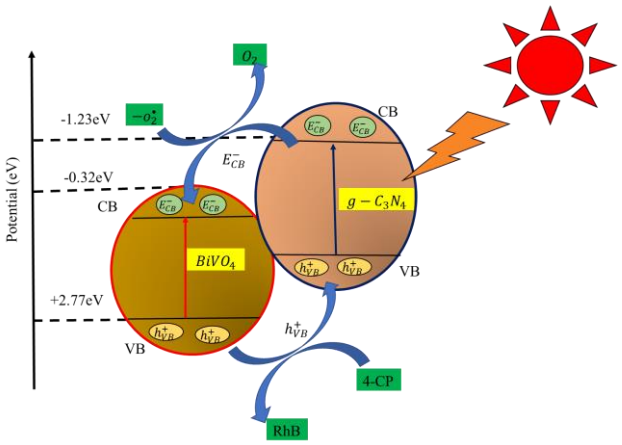

Fig. 2: Proposed mechanism of photocatalytic g-C3N4/ BiVO4 nanomaterial

3.3 Synthesis of ZnWO4 / g-C3N4 Nanomaterial

The $ZnWO_4$ nanomaterials have been produced using a facile hydrothermal method. At first, 1.65g of Na_2WO_4 & 0.85g of Zn $(NO3)_3.2H_2O$ were diluted with 50 ml of deionized water for 30 minutes with continuous stirring. Condensed NaOH was added to the solvent to change pH, [31]. The suspension was placed in a Teflon-lined stainless-steel autoclave at 150oC for 12 hours and cooled naturally. The pale-yellow solid was rinsed with 20ml of ethanol, water, and acetone before drying overnight in a desiccator at 80oC under a 10-2 bar vacuum. We subsequently got pure ZnWO4 powder suspension, [32]. After mixing the g-C3N4 with methanol, it is aggressively agitated for 1 hour to disperse. Drying the dispersion at 80oC and calcining at 300oC for 4 hours generates heat energy to join ZnWO4 and g-C3N4, resulting in a photocatalyst with different weight ratios. The weighted ratio of the g-C3N4 and $ZnWO_4$ materials is 1:1, 2:1, and 3:1. These samples are labeled GZW1, GZW2, and GZW3 (Figure 2).

3.3.1 Photocatalytic Setup

This suspension was treated under an Xe lamp equipped with a photocatalyst. Before UV-vis spectroscopy measurement, all dispersions were centrifuged to eliminate the residual nanoparticles and measure the degradation efficiency of dyes using a pseudo-first-order kinetics model, [33]. First, the initial rate of Elimination of COD is computed as follows:

$$Ro = -dK/Dt \quad (29)$$

Ro is the COD concentration K rate at t time. the data rate can be modulated first order kinetics as follows:

$$R = D_{app} * K \quad (30)$$

where t time and D_{app} denote apparent first-order rate constant using boundary condition $K = K_o$ at t = 0 gives:

$$\ln\frac{K_t}{K_0} = -D_{app} * t \quad (31)$$

The variation in their composite ratio further confirms their behavior. Moreover, the g-C_3N_4 and $ZnWO_4$ ratios have been adjusted to 4:1 and 5:1, including both, and symbolized as GZW4 and GZW_5, respectively. GZW_1, GZW_2, GZW_3, GZW_4, and GZW_5 degradation increased efficiency are 44, 72, 98, 85, and 7, respectively

3.3.2 Photocatalytic Mechanism

The ZnWO4 / g-C3N4 photocatalyst mechanism When exposed to visible light, g-C3N4 is quickly excited, and electron-hole pairs form on its surface. Because of its wide bandgap, excitation by visible light is prohibited in ZnWO4, [34]. The photoinduced active radicals OH and h+ were found to be beneficial for the degradation of 4-CPand RhB, and they are as follows:

$$hv + ZnWO_4 / g\text{-}C_3N_4 \rightarrow ZnWO_4 / g\text{-}C_3N_4 (E_{CB}^{-} + h_{VB}^{+}) \quad (32)$$

$$O_2^{-} \leftarrow O_2 + ZnWO_4 (E_{CB}^{-}) \quad (33)$$

$$H_2O_2 \leftarrow 2ZnWO_4 (E_{CB}^{-}) + O_2 + 2H^{+} \quad (34)$$

$$H_2O_2 + O_2^{-} \rightarrow OH + OH^{-} + O_2 \quad (35)$$

$$Dye + g\text{-}C_3N_4(hv_{VB}^{+}) \rightarrow P_{OXIDATION} \quad (36)$$

$$Dye + OH \rightarrow P_{DEGRADATION} \rightarrow CO_2 + H_2O \quad (37)$$

$$Dye + O_2^{-} \rightarrow P_{REDUCTION} \quad (38)$$

These findings suggest that the heterostructured nanocomposite's solid interfacial interactions would improve the transfer mechanism and reduce photoinduced charge carrier reunification, improving the g-C_3N_4/$ZnWO_4$nanocomposite's visible-light performance, [35].

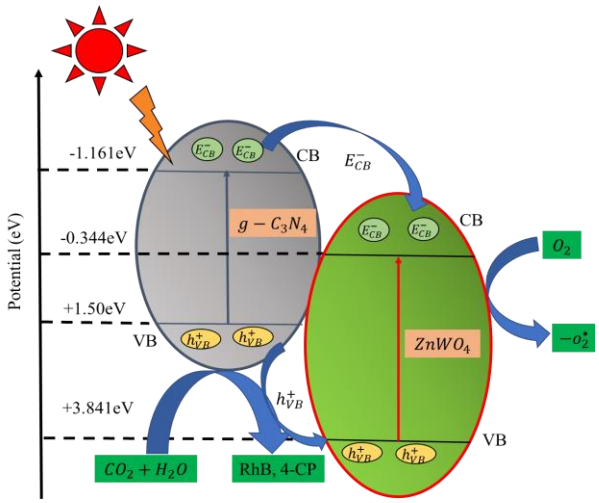

Fig. 3: Photocatalytic degradation of pollutants in g-C_3N_4/ ZnWO4 nanomaterial

3.4 Synthesis of CuWO4 / g-C3N4 Nanomaterial

The facile hydrothermal route also prepares the CuWO4 nanomaterials. The suspension of pure CuWO4 powder was obtained. Initially, 0.3g of Na2WO4 and 0.3 g of Cu (NO3)2 are mixed under magnetic stirring for 1 hour until becoming sky blue suspension. The yellowish-green solid is frequently washed with ethanol and distilled water. Then, the particular quantity of g-C3N4 is lent to methanol, which is stirred ultrasonically for 1 hour to disperse the g-C_3N_4. After drying at 80°C for002012 h and then calcining at 300°C for 4 hours to connect $CuWO_4$ and g-C_3N_4 samples, the photocatalyst with different g-C_3N_4 weight ratios is obtained. The weighted ratio of the g-C3N4 and $CuWO_4$ materials is 1:1, 2:1, and 3:1, and These samples are labeled as GCuW1, GCuW2, and GCuW3 (Figure 3), [36].

3.4.1 Photocatalytic Setup

RhB and 4-CP degrade 88% within 100 minutes. As CuWO4 loading rises, deterioration efficiency decreases. The enhanced agglomeration of CuWO4 nanoparticles may be interfering with electron transport from $CuWO_4$ / g-C_3N_4. Kinetic diagrams indicate linearity as

$$K = \ln(C_0/C) \quad (39)$$

The illumination duration affirms that the degradation reaction may follow first-order kinetics.

3.4.2 Photocatalytic Mechanism

The removal of toxic pollutants by the synthesized $CuWO_4$ / g-C_3N_4 photocatalysts is performed under the UV-vis spectrometer under dark and light illumination. Initially, the electron and hole separation from the $CuWO_4$ is as follows,

$$hv + CuWO_4 / g\text{-}C_3N_4 \rightarrow CuWO_4 / g\text{-}C_3N_4 (E_{CB}^- + h_{VB}^+) \quad (40)$$

The band potential of $CuWO_4$ / g-C_3N_4 was 2.41 eV and 0.28eV for the valance band and conduction band, respectively.

$$h_{VB}^+ + H_2O \rightarrow OH^{\bullet} + H_{VB}^+ \quad (41)$$

$$O_2^{\bullet -} \leftarrow O_2 + E_{CB}^- \quad (42)$$

$$h_{VB}^+ + OH^- \rightarrow HO^{\bullet} \quad (43)$$

$$O_2^{\bullet -} + H_2O \leftarrow O_2H^{\bullet} + OH^- \quad (44)$$

$$2O_2H^{\bullet} \rightarrow H_2O_2 \quad (45)$$

$$H_2O_2 + \rightarrow 2OH^{\bullet} \quad (46)$$

The procedure for RhB and 4-CP degradation by the synthesized $CuWO_4$ / g-C_3N_4 photocatalysts under vis light is expressed as follows:

$$\text{Dye} + \text{g-}C_3N_4(hv_{VB}^+) \rightarrow P_{OXIDATION} \quad (47)$$

$$\text{Dye} + OP_{DEGRADATION}H \rightarrow \rightarrow CO_2 + H_2O \quad (48)$$

$$\text{Dye} + O_2^- \rightarrow P_{REDUCTION} \quad (49)$$

The band energies better understand the improved performance of the photocatalytic of CuWO4 / g-C3N4 nanomaterials, [37].

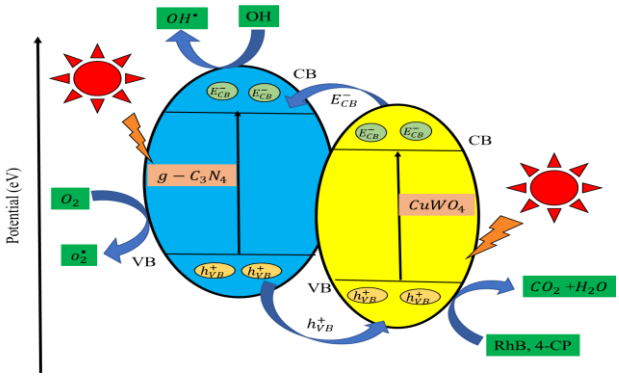

Fig. 4: Proposed mechanism of g-C3N4/ CuWO4 nanomaterial

3.5 Photocatalytic Efficiencies

The Nanoparticle photocatalysts present heterogeneous structure, energy, and function characteristics at spatial and temporal scales (Figure 4).

3.5.1 Enhanced Reaction and Diffusion Mathematical Statement

A reaction-diffusion equation consists of two terms: a reaction and a diffusion, and its standard form is as follows:

$$u_t = D\Delta u + f(u) \quad (50)$$

The Laplace operator is being shown. The volume or concentration of a substance, a species, etc., at point x R n at period interval is expressed by the parameter value u = u(x,t) (is an infinite set). Δ Consequently, "diffusion" is stated in the initial phrase on the privilege, which also incorporates D as the diffusion coefficient, [38]. The second derivative, f(u), is a continuous non-linear function: R R and represents occurrences that really "alter" the current u, i.e., whatever occurs to it (creation, mortality, chemical processes, etc.), as as opposed to simply allowing it to diffuse in the context (Figure 5).

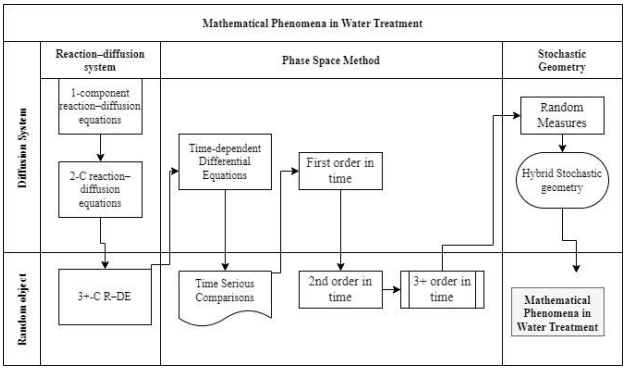

Fig. 5: Hybrid Stochastic Geometry Mathematical Model in Water Treatment

This session will explore defensive response solutions analytically and identify more practical uses against the Mathematical Phenomena in Water Treatment. This research also included the Phase Space Method for creating and studying dynamic system solutions. This will react with the help of Phase Space with dynamical system theory, [39].

3.5.2 Combined Phase Space Method

We combined the Phase Space Method with the Stochastic geometry and the Phase Space model. This helps to handle serious time problems, [40]. The phase space method is used in applied mathematics to build and analyze dynamical system solutions—that is, to resolve time-dependent differential equations, [41]. The Phase space is defined as a set of all physical states in classical mechanics. Therefore, the phase space is two-dimensional: position and momentum, in a one-dimensional system like a ball thrown directly up or a spring, [42]. The phase space has six trillion dimensions, three locations, and three momenta for each particle for a trillion particles in a three-dimensional box. System: when we refer to a "state," we don't just mean the locations of all the objects. A system, but also they're (which would need physical or configuration space)—moments or velocities that would occupy momentum space.

3.5.3 Hybrid Stochastic Geometry

Hybrid Stochastic geometry combines the Combined Phase Space Method with the Stochastic geometry model. In this era, stochastic geometry is combined with the Phase Space Method and Reaction & Diffusion derivation for executing the 1-component reaction-diffusion equations, 2-component reaction-diffusion equations, and 3-component reaction-diffusion equations. This Diffusion derivation gives the Time-dependent Differential Equations concerning the Time Serious Comparisons, [43]. Hence, the Time Serious Comparisons in stochastic geometry are explained below.

3.6 Bayesian Structural Time Series Technique

Forecasting and pattern identification may be utilized to enhance the Bayesian Structural Time Series (BSTS) approach to estimate harmful pollutant degradation utilizing photocatalysts. Analysis was done on toxic pollutant degradation over 100 minutes. The four photocatalysts may be analyzed using irradiation time data. The Bayesian posterior sampling distributions BSTS package was used with R software, [44]. Photocatalytic mechanism priors can be effectively integrated with Bayesian structural models. Applying established concepts to the model, presents an effective approach to streamlining a substantial array of interconnected variables into a more concise framework. Furthermore, the model considers the uncertainty associated with the coefficient estimates when producing the credible interval for the predictions, employing priors on the regressor coefficients.

We can modify the mathematical expression for the degradation rate by introducing additional parameters to represent the effect of the different photocatalysts. Let k_i be the rate constant for the degradation of the pollutant using photocatalyst i.

Then, we can write:

$$\frac{dC}{dt} = -\sum_i (k\_i)C \tag{51}$$

The sum is taken over all photocatalysts, and the negative sign indicates that the concentration of the pollutant decreases with time, and the decay rate is proportional to the concentration. Then we can write:

$$\frac{dC}{dt} = -\sum_i (k\_1\ g - C_3N_4/MnWO_4 + k\_2\ g - C_3N_4/MnWO_4 + k\_3\ g - C_3N_4/MnWO_4 + k\_4\ g - C_3N_4/MnWO_4)C \quad (52)$$

where the rate constant for each photocatalyst is multiplied by the type of photocatalyst. To incorporate the effect of time and other covariates, we can use a BSTS model as follows:

$$y\_t = \beta(x\_t) + \eta\_t + \varepsilon\_t \quad (53)$$

where y_t is the degradation rate of the toxic pollutant at time t, x_t is a vector of covariates that may affect the degradation rate, such as the concentration of the photocatalyst or environmental factors, β is a vector of regression coefficients, η_t is a stochastic process that captures the temporal variation in the degradation rate, and ε_t is a Gaussian error term, [45]. We can use Bayesian inference to estimate the parameters of the BSTS model.

The model's parameters can be estimated using Bayesian inference, allowing us to make probabilistic forecasts of the degradation rate at irradiation time points. The strength of the photocatalyst $MnWO_4$, $BiVO_4$, $ZnWO_4$, and $CuWO_4$ with the same semiconductors, g-C_3N_4, is determined. By comparing another photocatalyst, the random error of the $ZnWO_4$ model does not exceed 3-4%, and the results of approximating the experimental values of the strength with Nano semiconductors with photocatalysts can be considered entirely satisfactory.

4 Result and Discussion

In the context of surface water pollution, MnWO4/g-C3N4, BiVO4/g-C3N4, ZnWO4/g-C3N4, and CuWO4/g-C3N4 are all types of photocatalysts that can be used to degrade pollutants in water. These materials absorb light and produce reactive oxygen species that can break down pollutants into harmless byproducts. 4-chlorophenol and Rhodamine B are both common pollutants found in surface water ecosystems. 4-chlorophenol is a toxic chemical that is often used in industrial processes. At the same time, Rhodamine B is a fluorescent dye used in various applications. To study the impact of these pollutants on surface water ecosystems, researchers can use different techniques to model the distribution of contaminants in a given area.

The pollutant's concentration, influences the degradation rate. From the proposed system, we take the photocatalytic measurements as a first-order kinetic reaction of toxic pollutants for the photocatalyst samples, cycling stability test as degradation efficiency. The performance of four catalysts was compared based on the factors, namely high rate constant K(m^{-1}), correlation coefficient (R^2), and degradation efficiency values of photocatalysts.

The degradation rate initially increases rapidly with increasing irradiation time as more photocatalytic active sites become available and the reaction rate increases. At the same time, as the reaction progresses and the pollutant concentration decreases, the degradation rate eventually levels off and approaches a plateau. This plateau is often called the steady-state degradation rate, representing the maximum rate achievable with a particular photocatalyst under specific reaction conditions. In summary, the photocatalytic degradation rate of a target pollutant generally increases with irradiation time, and a pseudo-first-order kinetic reaction can describe the relationship between them. The analysis of the performance of MnWO4/g-C3N4 using kinetic pseudo-first-order response is shown in Table 1 (Appendix).

From Figure 1, for RhB, After 40 minutes of irradiation, the degradation rate constant of $MnWO_4$ and GMW_3 towards 0.0152 m^{-1} and 0.0251 m^{-1}. After 100 minutes of irradiation, the degradation rate constant was 0.0194 m^{-1} and 0.0142 m-1 for $MnWO_4$ and GMW_3. The photocatalytic degradation rate of RhB using a GMW_3 composite photocatalyst was highly dependent on the irradiation time. Figure 2 compares MnWO4 and GMW3 for the 4-CP pollutant degradation. After 40 minutes of irradiation, the degradation rate constant was 0.0098 m-1 and 0.0132 m-1 for GMW_3 and $MnWO_4$. After 100 minutes of irradiation, the degradation rate constant of GMW_3 and $MnWO_4$ was 0.0055 m^{-1} and 0.078 m-1. The photocatalytic degradation rate of 4-CP and RhB using different composite photocatalysts also increased with increasing irradiation time. After 100 minutes of irradiation, the degradation rate reached 97% for RhB and 4-CP 92%. The GMW_3 catalyst has a higher rate constant of 0.084 m-1 than the $MnWO_4$ constant of 0.0504 m^{-1}.

Decolorizing dyes in the water source is an essential process for wastewater management. In the photocatalytic degradation of dyes, COD analysis can be used to evaluate the efficiency of the photocatalytic process in mineralizing the dye molecules into more straightforward and less harmful compounds, as displayed in Table 2 (Appendix). We estimate the photocatalyst's high

catalytic nature using chemical oxygen demand efficiency measures in terms of percentage.

The efficiency of photocatalytic degradation of dyes RhB and 4-CP can be evaluated using COD analysis. Figure 3 and Figure 4 show the COD removal efficiency increased with increasing reaction time for different photocatalysts. The COD removal efficiency for RhB using MnWO4 photocatalyst was 68.7% after 100 minutes of irradiation, while the GMW3 photocatalyst had higher COD than the other sample photocatalyst after 100 minutes of irradiation. After 100 minutes of irradiation, the COD removal efficiency for 4-CP using the g-C3N4/MnWO4 composite photocatalyst was found to have lesser COD removal efficiency than the GMW3. From the observance of Figure 3, the GMW3 has the highest decolorisation of RhB dye at 92%, and according to Figure 4, the GMW3 has the highest decolorisation of 4-CP dye at 86%. Then, the degradation efficiency for MnWO4 and GMW3 will be estimated to analyze which photocatalyst has the highest performance in pollutant degradation as displayed in Table 3.

Table 3. The degradation efficiency of visible light photoactivity

Cycle number	Degradation Efficiency(%)			
	RhB		4-CP	
	MnWO4	GMW3	MnWO4	GMW3
1	35	95	34	89
2	38	96	36	88
3	39	94	37	89
4	38	96	35	90
5	37	97	36	88

Figure 5 shows that both $MnWO_4$ and GMW_3 photocatalysts exhibited degradation efficiency for RhB and 4-CP even after multiple cycles of photocatalysis. Initially, the $g\text{-}C_3N_4$ and $MnWO_4$ have poor degradation efficiency at 33% and 35% of RhB, respectively. Similarly, the $g\text{-}C_3N_4$ and $MnWO_4$ display poor degradation efficiency for 4-CP dye at 32% and 34%, respectively. For GMW_3, the degradation efficiency for 4-CP was found to be 89% after the first cycle of photocatalysis and decreased to 88% after the fifth cycle of photocatalysis. After 100 minutes of light irradiation, the GMW_3 has a 97% degradation efficiency of RhB. The degradation efficiency of the 4-CP dye for GMW_3 is 92%. Because the GMW3 weights g-C3N4:MnWO4 has a 3:1 ratio that influences the separation of electron-hole pair, improving its efficiency. The study concluded that GMW_3 photocatalysts exhibited good stability and reusability for the photocatalytic degradation of RhB.

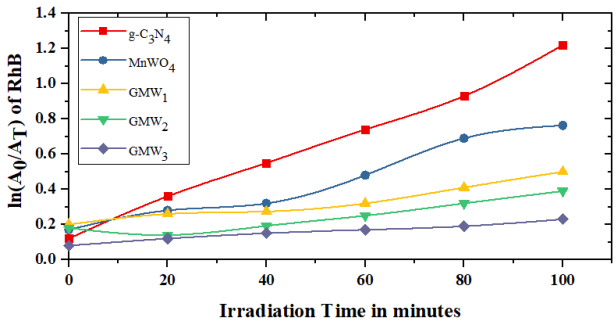

Fig. 6: Effect of photocatalysts on kinetic plot degradation rate constant of RhB

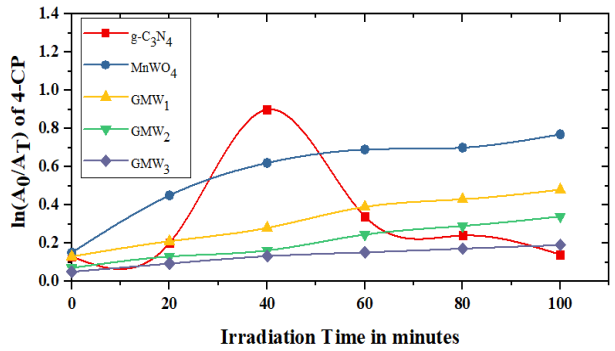

Fig. 7: Effect of different photocatalysts on kinetic plot degradation rate constant of 4-CP

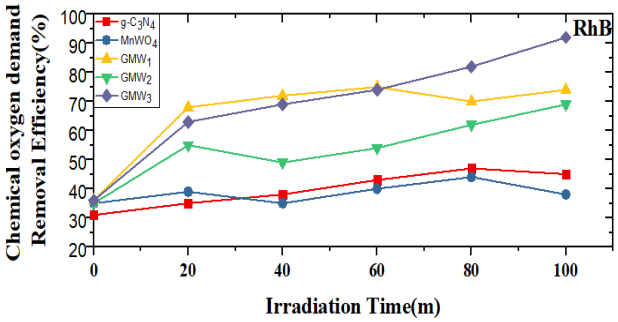

Fig. 8: The chemical oxygen demand of RhB by different photocatalysts with increasing irradiation time

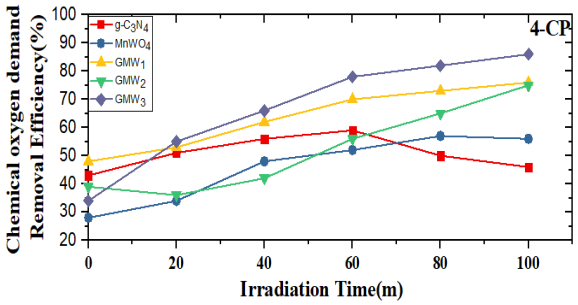

Fig. 9: The COD of 4-CP by photocatalysts is based on the irradiation time

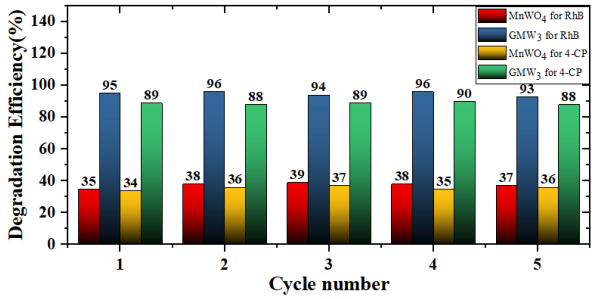

Fig.10: Comparison of degradation efficiency of RhB and 4-CP by $MNWO_4$ and GMW_3 photocatalysts

Overall Figure 8, Figure and Figure 10, the GMW_3 photocatalyst shows a higher degradation efficiency, rate constant, and long-term stability measure for dyes. Under visible light irradiation, the GMW_3 photocatalyst has 97% and 92% degradation efficiency for RhB and 4-CP dyes. The GMW_3 has a degradation rate constant of 0.0942(m^{-1}) and long stability for RhB; similarly, GMW_3 has a degradation rate of 0.0504(m^{-1}) for 4-CP dye.

Then, take the bare g-C_3N_4 and $BiVO_4$ as photocatalysts treated under visible light irradiation for up to 100 minutes with an interval of 20 minutes. Initially, the photocatalyst $BiVO_4$ had lower degradation efficiency of 28% and 34% towards the dyes RhB and 4-CP. Then, we add the BiVO4 into g-C3N4 in different ratios, which may improve the degradation efficiency performance. The bare g-C3N4 also has a lower degradation efficiency of dyes. The maximum degradation efficiency for dyes RhB and 4-CP is attained by 89% and 94% using a GBV3 catalyst sample. Then, the degradation rate is determined using pseudo-first-order kinetic reaction for different photocatalysts, as displayed in Table 4 (Appendix).

The first kinetic relation was found to be linear, determined from the slope of the linear plot in Figure 6 and Figure 7 of $\ln.\frac{K_t}{K_0}$ Versus irradiation time. After 100 minutes of irradiation, for Rhb, the higher rate constant of g-C3N4, $BiVO_4$, GBV_1, GBV_2, and GBV_3 as 0.32 m^{-1}, 0.60 m^{-1}, 0.94 m^{-1}, 1.54 m^{-1} and 1.81 m^{-1} respectively. similarly, for 4-CP , the g-C3N4, $BiVO_4$, GBV_1, GBV_2, and GBV_3 towards 0.43m^{-1}, 0.87m^{-1}, 0.92 m^{-1}, 1.59m^{-1} and 2.26m^{-1}. from this, the GBV_3 has a higher rate constant of 0.0821m^{-1} and 0.0643m^{-1} of RhB and 4-CP that is higher than the 0.0221m^{-1} and 0.0221m^{-1} of $BiVO_4$ photocatalysts of RhB and 4-CP dyes. The Chemical Oxygen Demand (COD) measures the amount of organic matter in a water sample that a strong chemical oxidant can oxidize. It often indicates the degree of pollutant RhB and 4-CP in water samples captured approximately in Table 5 (Appendix).

The comparison analysis of the COD removal efficiency of Rhodamine B (RhB) and 4-CP dye using a different photocatalyst under visible light irradiation is shown in Figure 13 and Figure 14. The study found that both photocatalysts exhibited high COD removal efficiencies for RhB dye. The higher the COD value, the higher the number of organic pollutants in the water. For the g-C3N4/BiVO4 photocatalyst, the COD removal efficiency for RhB dye was 65% after 100 minutes of irradiation under visible light. For the GMW_3 photocatalyst, the COD removal efficiency for RhB dye was 86% after 100 minutes of irradiation under visible light.
Similarly, for 4-chlorophenol (4-CP) dye, the GMW_3 photocatalysts exhibited high COD removal efficiencies. The higher COD removal efficiency of GMW_3 photocatalysts than the other photocatalysts can be attributed to the larger specific surface area and multiple active sites for photocatalytic degradation. Overall, the study found that GMW_3 photocatalysts were more effective for the COD removal of RhB and 4-CP dyes under visible light irradiation than the other photocatalysts.

Table 6. The degradation efficiency of $BiVO_4$ and GBV_3

Cycle number	Degradation Efficiency(%)			
	RhB		4-CP	
	$BiVO_4$	GBV_3	$BiVO_4$	GBV_3
1	28	85	34	92
2	27	87	35	89
3	29	89	33	90
4	28	84	37	88
5	27	83	38	87

Figure 11 and Figure 12 compare the RhB and 4-CPdyes degradation efficiency using $BiVO_4$ and GBV_3 with the stability test performed up to five cycles, and its measures are observed and shown in Table 6. At the first cycle of the photocatalysis, the estimated degradation efficiency of RhB for $BiVO_4$ and GBV_3 has values between 28% and 85%. Similarly, for 4-CP, 34% and 92% for $BiVO_4$ and GBV_3, respectively, The cycles are increased up to 5, and the degradation of dyes percentage also increased gradually; in 3rd cycle, test analysis shows poor degradation efficiency of dyes RhB and 4-CP of 29% and 33 with the $BiVO_4$ photocatalyst. At the same time, the GBV_3 catalyst has 89% and 90% better degradation efficiency for dyes RhB and 4-CP, respectively. Figure 15 shows that the 3:1 ratio of the g-C_3N_4/ $BiVO_4$ sample as GBV_3 photocatalyst

has better degradation efficiency than the pure $BiVO_4$ photocatalyst. The photocatalytic shows that the direct oxidation effect analyses dyes' degradation. Overall, GBV_3 has enough catalytic stability and cost-effective visible light photocatalyst for pollutant reduction in surface water.

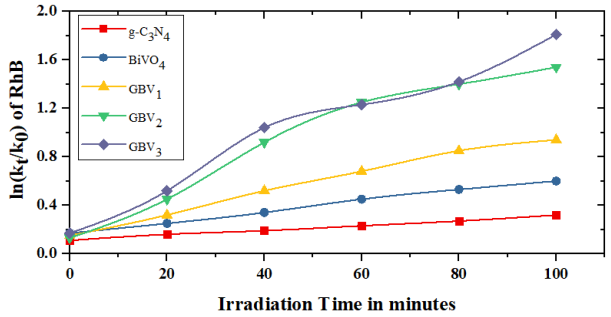

Fig. 11: The kinetic plot degradation of RhB dye with a different weight ratio of photocatalyst

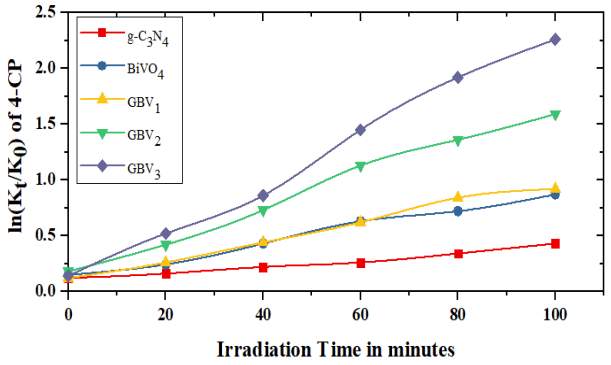

Fig. 12: The kinetic plot degradation of 4-CP dye with the different weight ratio of photocatalyst

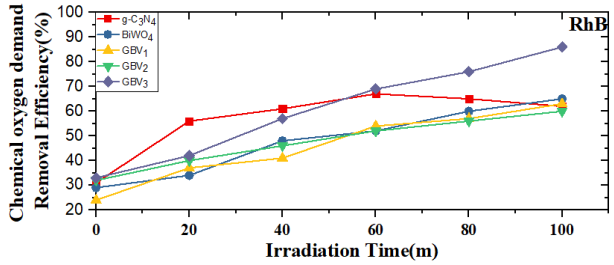

Fig. 13: The photocatalytic COD removal efficiency of RhB dye based on irradiation time

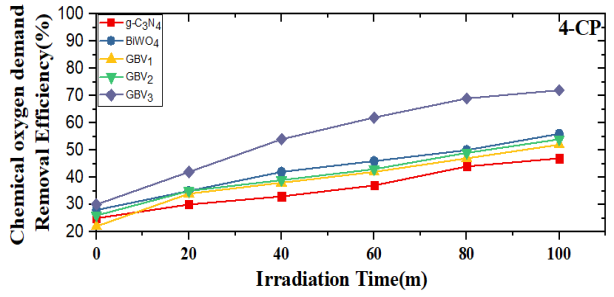

Fig. 14: The photocatalytic COD removal efficiency of 4-CP dye versus Irradiation time minutes

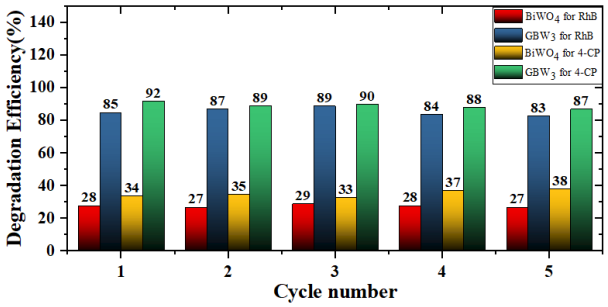

Fig. 15: The comparison analysis of two photocatalysts degradation efficiency of two pollutants

The different photocatalysts g-C3N4/ZnWO4 is monitored under visible light irradiation to degrade pollutants such as RhB and 4-CP. The first-order kinetic reaction for the g-C3N4/ZnWO4 photocatalytic degradation of RhB and 4-CP was measured and shown in Table 7 (Appendix).

Figure 16 and Figure 17 show a kinetic plot relationship of the different sample photocatalysts based on the irradiation time. The degradation rate of RhB and 4-CP dyes by g-C_3N_4, $ZnWO_4$, GZW_1, GZW_2, and GZW_3 photocatalysts may vary with irradiation time. In general, increasing the irradiation time may lead to an increase in the degradation rate of the dyes. This is because the photocatalyst can absorb more photons, leading to more electron-hole pairs and, consequently, more reactive species that can degrade the dyes. The photocatalyst's properties and the dye molecules' nature may also influence the degradation rate of RhB and 4-CP dyes. For instance, the adsorption capacity of the photocatalyst for the dye molecules may affect the degradation rate. For the GZW_3 catalyst, the high constant rate of the RhB and 4-CP are 0.0914(m^{-1}) and 0.0731(m^{-1}), which is 4.10 times and 6.3 times better than the $ZnWO_4$ catalyst. From the observance of Figure 18 and Figure 19, the optimal irradiation time for achieving the highest degradation rate for the GZW_3 photocatalyst-RhB, 4-CP dye system.

The Chemical Oxygen Demand (COD) measures the oxygen required to oxidize organic matter in a water sample. Higher COD values indicate higher levels of organic matter and pollution in the water. The COD removal efficiency of various photocatalysts is shown in Table 8 (Appendix).

These studies suggest that GZW_3 may effectively eliminate COD from wastewater containing dyes, and the GZW_3 photocatalyst achieves higher decolorization efficiency at 97% and 85% towards the pollutant as RhB and 4-CP.

Table 9. The comparison between different weight photocatalysts for degradation efficiency of RhB and 4-CP dye

Cycle number	Degradation Efficiency(%)			
	RhB		4-CP	
	$ZnWO_4$	GZW_3	$ZnWO_4$	GZW_3
1	55	99	56	89
2	58	98	57	90
3	59	99	58	89
4	58	98	57	88
5	57	98	58	89

A sample of dye-containing wastewater would be treated with ZnWO4 and GZW3, and the COD of the treated wastewater would be measured. The cycle number would refer to the times the treatment was repeated using the same material. The degradation efficiency of ZnWO4 and GZW3 for RhB and 4-CP dyes as a function of cycle number is shown in Figure 20 and observed in Table 9.

$$\text{Degradation Efficiency (\%)} = \frac{\text{COD of untreated wastewater} - \text{COD of treated wastewater}}{\text{COD of untreated wastewater}} \text{x } 100 \quad (54)$$

At the same time, the degradation efficiency may decrease with each cycle as the treatment material becomes saturated with the dye and loses effectiveness.

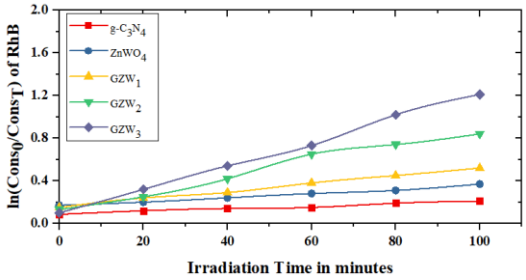

Fig. 16: The kinetic plot unsbscribe$\ln\frac{Cons_o}{Cons_T}$ relationship with the irradiation time of photocatalysts for RhB dye degradation

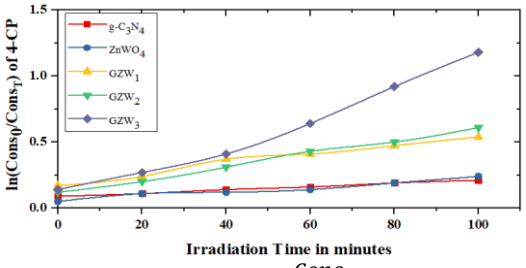

Fig. 17: The kinetic plot $\ln\frac{Cons_o}{Cons_T}$ relationship with the irradiation time of photocatalysts for 4-CP dye degradation

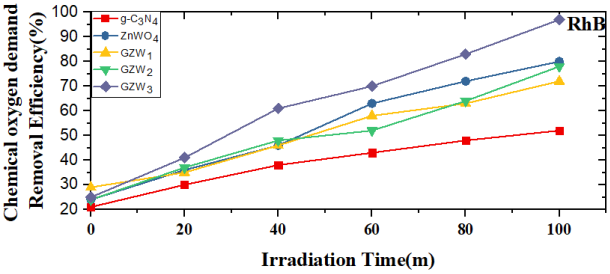

Fig. 18: The COD removal efficiency of RhB for photocatalysts under visible light irradiation

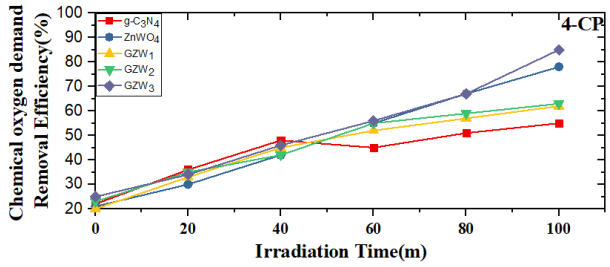

Fig. 19: The COD removal efficiency of 4-CP for photocatalysts under visible light irradiation

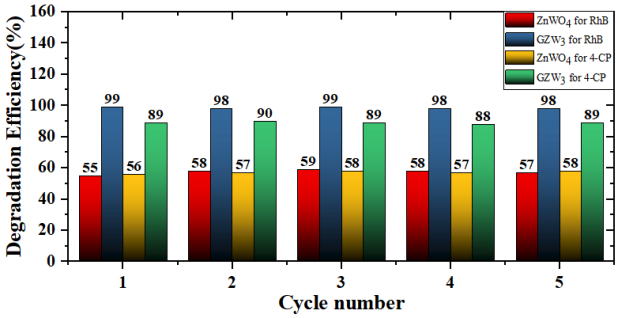

Fig. 20: Comparison between degradation efficiency of $ZnWO_4$ and GZW_3 over an increasing count of cycles

The g-C_3N_4/$CuWO_4$ composite material is treated under visible light, and it achieves degradation of 13% and 24% for RhB dyes after 100-minute irradiation. Similarly, the degradation of 4-CP dye using g-C_3N_4 and $CuWO_4$ is attained at 13% and 22%, respectively. After that, $CuWO_4$ is added to g-C_3N_4 in three different weight ratios; from that, the $GCuW_3$ has the highest photocatalytic activity, [46]. The photodegradation rate is measured using the first-order kinetic reaction model in Table 10 (Appendix).

Figure 21 and Figure 22 show that the kinetic degradation rate of a catalyst refers to the rate at which it can break down or degrade a particular pollutant as RhB (Rhodamine B) and 4-CP (4-Chlorophenol) are the target pollutants, and catalysts, g-C_3N_4, $CuWO_4$, $GCuW_1$, $GCuW_2$, and $GCuW_3$, are evaluated for their kinetic degradation rate. The g-C_3N_4 and CuWO4 nanoparticles showed

a high kinetic degradation rate for RhB, with a rate constant of 0.0032m^{-1} and 0.0041 $m^{-1,}$ respectively. For 4-CP, the rate constant of 0.0013 m^{-1}, 0.0014 m^{-1}respectively. The $GcuW_1$ and $GcuW_2$ had a higher kinetic degradation rate constant of 0.0047 m^{-1} and 0.0041 m^{-1}. For 4-CP, the rate constant was 0.0023 m^{-1} and 0.0027$m^{-1,}$ respectively. The $GCuW_3$ had a higher kinetic degradation rate for RhB than $CuWO_4$, with a rate constant of 0.0812 $m^{-1,}$ and for 4-CP, the rate constant was 0.0715 m^{-1}. From th above measures, both $CuWO_4$ and $GCuW_3$ have high kinetic degradation rates for RhB, with $GCuW_3$ showing slightly higher rates than $CuWO_4$. At the same time, the kinetic degradation rates for 4-CP are lower than those for RhB, and GCuW3 has higher rates than CuWO4.

In other words, the COD (Chemical Oxygen Demand) efficiency analysis measures a catalyst's ability to degrade or remove organic compounds from wastewater. In this case, the dyes RhB (Rhodamine B) and 4-CP (4-Chlorophenol) are the target pollutants, and two catalysts, ZnWO4 and GZW3, are being evaluated for their COD efficiency, which is displayed in Table 11 (Appendix).

Table 12 specifically investigates the degradation efficiency and Figurs 23 and Figure 24 show the COD efficiency of these catalysts for the degradation. The GCuW3 had a COD removal efficiency of 80% for RhB after 100 minutes of reaction time.

Table 12. The degradation efficiency at different cycles

Cycle number	Degradation Efficiency(%)			
	RhB		4-CP	
	$CuWO_4$	$GCuW_3$	$CuWO_4$	$GCuW_3$
1	25	88	29	89
2	28	86	26	88
3	29	89	27	89
4	28	86	25	90
5	27	87	26	88

Figure 25 shows the CuWO4 and $GCuW_3$ photocatalysts used in wastewater treatment for dyes, with their efficiency in degrading RhB and 4-CP dyes. After one cycle of photocatalysis, the $CuWO_4$ and $GcuW_3$ remove the dyes 25% and 88% for RhB, and for 4-CP, the photocatalyst $CuWO_4$ and $GcuW_3$ has degradation efficiency of dyes 29% and 89%. After five treatment cycles, the $CuWO_4$ and $GcuW_3$ were effective at removing RhB dye with % degradation efficiency of 27% and 87%. Similarly, removing the RhB dye of $CuWO_4$ and $GcuW_3$ has a degradation efficiency of 26% and 88%. The degradation efficiency is reduced when the loading amount of $CuWO_4$ increases because the excess CuWO4 particle did not favor the electron transfer from the g-C_3N_4/ $CuWO_4$. From these results, the $GCuW_3$ outperforms the other photocatalysts, [47].

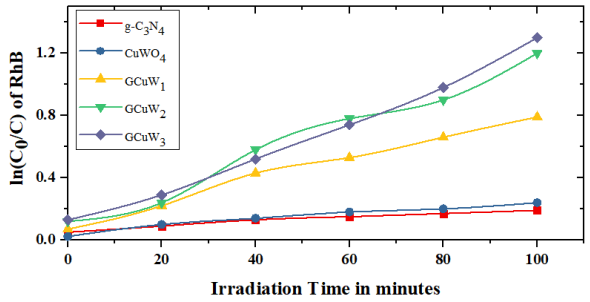

Fig. 21: The kinetic plot of degradation of RhB dye using different concentrations of g-C_3N_4/$CuWO_4$ based on the irradiation time

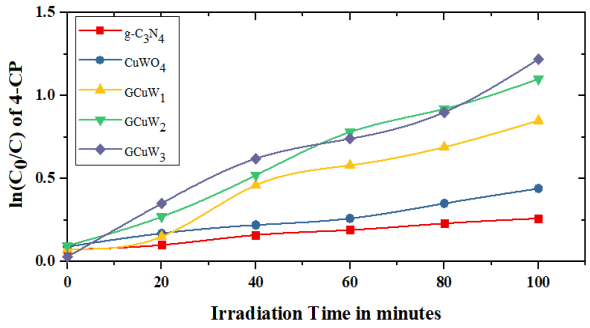

Fig. 22: The kinetic plot of degradation of 4-CP dye using different concentrations of g-C_3N_4/$CuWO_4$ based on the irradiation time

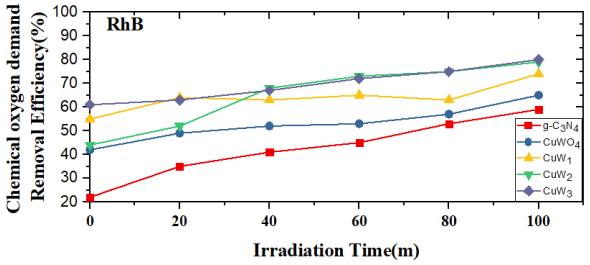

Fig. 23: COD removal efficiency for RhB dye

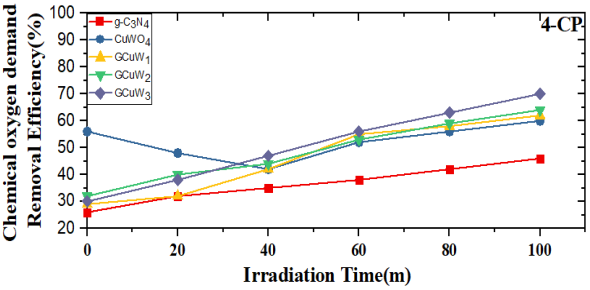

Fig. 24: The COD removal efficiency of different photocatalysts for 4-CP dye

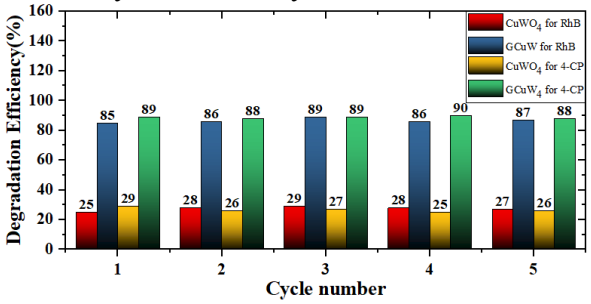

Fig. 25: Comparison analysis of degradation efficiency over cycles

Overall Figure 25, the different weights of photocatalytic show better activity for the RhB and 4-CP dyes. In the degradation process, the doses of photocatalysts play a crucial role that may affect the degradation rate of pollutants. From Table 13 (Appendix), the higher degradation rate of RhB dye is achieved by the g-C_3N_4/ $ZnWO_4$ photocatalyst than the other photocatalyst, [48]. From this measure, we can say that the g-C3N4/ ZnWO4 photocatalyst overperforms the other photocatalyst, making it more suitable for surface water treatment.

5 Conclusion

This research focused on the mathematical modeling of the essence of the effects and the pollution based on favorable factors to evaluate and solve the problems associated with the growth of pollutants in the surface water ecosystem. Moreover, the model of Stochastic geometry, Reaction and Diffusion, Phase Space Method, and Time Series technique model for enabling the reduction of the Pollutants in the Surface Water Ecosystem to produce the stability of the environment and the pollution in the atmosphere was evaluated. The accurate result of global stability of the parameters of level 1 produces higher stability. The calculation of This parameter uses the Different instances of international equilibrium. Meanwhile, the measurement of global non-linear stability of the parameters of level -2 enhances global solutions against the time series parameter. This result gives on the contamination status of pollutants in surface water and its respective ecosystem sources, and potential risks of environmental regulation were active green innovation against pollution reduction.

Declaration of Generative AI and AI-assisted Technologies in the Writing Process

The authors wrote, reviewed and edited the content as needed and they have not utilised artificial intelligence (AI) tools. The authors take full responsibility for the content of the publication.

References:

[1] Xinbo Liu; Li Guo; Xihong Cui; John R. Butnor; Elizabeth W. Boyer; Dedi Yang., "An Automatic Processing Framework for In Situ Determination of Ecohydrological Root Water Content by Ground-Penetrating Radar," in *IEEE Transactions on Geoscience and Remote Sensing*, vol. 60, pp. 1-15, 2022, Art no. 4501715. doi: 10.1109/TGRS.2021.3065066.

[2] Sulabh Srivastava; Lalit Singh; Vishal Kaushik; Swati Rajput; Sourabh Jain; Manoj Kumar Pal; Mukesh Kumar., "Electrically Controlled Nanophotonic Slot Structure Based on Photocatalytic Nanocomposite for Optical Detection of Foodborne Pathogens," *in Journal of Lightwave Technology*, vol. 39, no. 20, pp. 6670-6677, Oct.15, 2021. doi: 10.1109/JLT.2021.3104409.

[3] Anh, H. Q., Le, T. P. Q., Da Le, N., Lu, X. X., Duong, T. T., Garnier, J., & Nguyen, T. A. H. (2021). Antibiotics in surface water of East and Southeast Asian countries: A focused review on contamination status, pollution sources, potential risks, and future perspectives. *Science of The Total Environment*, vol No 764, pp.142865. DOI: 10.1016/j.scitotenv.2020.142865.

[4] Rakib, Md. R. J., Jolly, Y. N., Begum, B. A., Choudhury, T. R., Fatema, K. J., Islam, Md. S.,Idris, A. M. (2021). Assessment of trace element toxicity in surface water of a fish breeding river in Bangladesh: a novel approach for ecological and health risk evaluation. *Toxin Reviews,* 41(2), pp 420–436. https://doi.org/10.1080/15569543.2021.1891936.

[5] Ng, B., Quinete, N., Maldonado, S., Lugo, K., Purrinos, J., Briceño, H., & Gardinali, P. (2021). Understanding the occurrence and distribution of emerging pollutants and endocrine disruptors in sensitive coastal South Florida Ecosystems. *Science of The Total Environment*, Vol.757, 143720. DOI: 10.1016/j.scitotenv.2020.143720

[6] Hairom, N. H. H., Soon, C. F., Mohamed, R. M. S. R., Morsin, M., Zainal, N., Nayan, N.,

& Harun, N. H. (2021). A review of nanotechnological applications to detect and control surface water pollution. *Environmental Technology & Innovation,* Vol.24, 102032. https://doi.org/10.1016/j.eti.2021.102032.

[7] Yang, Q., Gao, D., Song, D., & Li, Y. (2021). Environmental regulation, pollution reduction and green innovation: The case of the Chinese Water Ecological Civilization City Pilot policy. *Economic Systems*, Vol. 45(4), 100911. https://doi.org/10.1016/j.ecosys.2021.100911.

[8] Shakhman, I., & Bystriantseva, A. (2021). Water Quality Assessment of the Surface Water of the Southern Bug River Basin by Complex Indices. *Journal of Ecological Engineering*, Vol. 22(1):195-205 https://doi.org/10.12911/22998993/128858.

[9] Hamid Dashti; Nancy F. Glenn; Susan Ustin; Jessica J. Mitchell; Yi Qi; Nayani T. Ilangakoon; Alejandro N. Flores; José Luis Silván-Cárdenas; Kaiguang Zhao; Lucas P. Spaete; Marie-Anne de Graaff., "Empirical Methods for Remote Sensing of Nitrogen in Drylands May Lead to Unreliable Interpretation of Ecosystem Function," in *IEEE Transactions on Geoscience and Remote Sensing*, vol. 57, no. 6, pp. 3993-4004, June 2019. doi: 10.1109/TGRS.2018.2889318.

[10] Y. Jia, B. W. Lee and C. Liu, "Magnetic ZnFe2O4 Nanocubes: Synthesis and Photocatalytic Activity With Visible Light/H2O2," in *IEEE Transactions on Magnetics*, vol. 53, no. 3, pp. 1-5, March 2017, Art no. 2800305. doi: 10.1109/TMAG.2016.2640204.

[11] T. -L. Nguyen, T. N. Do and G. Kaddoum, "Performance Analysis of Multi-User NOMA Wireless-Powered mMTC Networks: A Stochastic Geometry Approach," in *IEEE Transactions on Communications*, vol. 70, no. 11, pp. 7400-7417, Nov. 2022. doi: 10.1109/TCOMM.2022.3214244.

[12] M. S. H. Khan, M. S. Islam, M. R. Islam, A. Iskanderani, I. M. Mehedi and M. T. Hasan, "Potential Visible-Light Driven PtO_2 /GaN vdW Hetero-Bilayer Photocatalysts for Water Splitting Using First-Principles," in *IEEE Access*, vol. 9, pp. 109510-109521, 2021. doi: 10.1109/ACCESS.2021.3102190.

[13] S. Wu, W. Zhou, K. Yan and X. Zhang, "Response of the Water Conservation Function to Vegetation Dynamics in the Qinghai–Tibetan Plateau Based on MODIS Products," in *IEEE Journal of Selected Topics in Applied Earth Observations and Remote Sensing*, vol. 13, pp. 1675-1686, 2020. doi: 10.1109/JSTARS.2020.2984830.

[14] D. X. Hammer, R. J. Thomas, G. D. Noojin, B. A. Rockwell, P. K. Kennedy and W. P. Roach, "Experimental investigation of ultrashort pulse laser-induced breakdown thresholds in aqueous media," in *IEEE Journal of Quantum Electronics*, vol. 32, no. 4, pp. 670-678, April 1996. doi: 10.1109/3.488842.

[15] M. Zeng, J. Liu, R. Yu and M. Zhu, "Photocatalytic Activity of Magnetically Retrievable Bi2WO6/ZnFe2O4 Adsorbent for Rhodamine B," in *IEEE Transactions on Magnetics*, vol. 50, no. 11, pp. 1-4, Nov. 2014, Art no. 5200604. doi: 10.1109/TMAG.2014.2323343.

[16] Linna Chai; Haiying Jiang; Wade T. Crow; Shaomin Liu; Shaojie Zhao; Jin Liu; Shiqi Yang., "Estimating Corn Canopy Water Content From Normalized Difference Water Index (NDWI): An Optimized NDWI-Based Scheme and Its Feasibility for Retrieving Corn VWC," in *IEEE Transactions on Geoscience and Remote Sensing*, vol. 59, no. 10, pp. 8168-8181, Oct. 2021. doi: 10.1109/TGRS.2020.3041039.

[17] X. Yang, X. Liu and X. Wu, "Photocatalytic activity of ion-doped ZnO powders," in *IEEE Transactions on Dielectrics and Electrical Insulation*, vol. 22, no. 3, pp. 1497-1500, June 2015. doi: 10.1109/TDEI.2015.7116343.

[18] D. P. Smetaniuk, M. T. Taschuk and M. J. Brett, "Photocatalytic Titanium Dioxide Nanostructures for Self-Regenerating Relative Humidity Sensors," in *IEEE Sensors Journal*, vol. 11, no. 8, pp. 1713-1719, Aug. 2011. doi: 10.1109/JSEN.2010.2095416.

[19] G. Narayanan, G. Muhiuddin, M. S. Ali, A. A. Z. Diab, J. F. Al-Amri and H. I. Abdul-Ghaffar, "Impulsive Synchronization Control Mechanism for Fractional-Order Complex-Valued Reaction-Diffusion Systems With Sampled-Data Control: Its Application to Image Encryption," in *IEEE Access*, vol. 10, pp. 83620-83635, 2022. doi: 10.1109/ACCESS.2022.3194030.

[20] K. Shi, Y. Li, Y. Zhang, L. Li, H. Lv and K. Song, "Classification of Inland Waters Based on Bio-Optical Properties," in *IEEE Journal of Selected Topics in Applied Earth Observations and Remote Sensing*, vol. 7, no.

2, pp. 543-561, Feb. 2014. doi: 10.1109/JSTARS.2013.2290744.

[21] M. S. H. Khan, M. R. Islam, M. S. Islam, I. M. Mehedi and M. T. Hasan, "Tunable Photocatalytic Properties of Planar GaN/GeC Hetero-Bilayer: Production of H_2 Fuel," in *IEEE Access*, vol. 8, pp. 209030-209042, 2020. doi: 10.1109/ACCESS.2020.3037036.

[22] M. -K. Lee, T. -H. Shih and C. -M. Shih, "Highly Visible Photocatalytic Activity of Fluorine and Nitrogen Co-doped Nanocrystalline Anatase Phase Titanium Oxide Converted From Ammonium Oxotrifluorotitanate," in *IEEE Transactions on Nanotechnology*, vol. 6, no. 3, pp. 316-319, May 2007. doi: 10.1109/TNANO.2007.894836.

[23] C. Wattanawikkam and W. Pecharapa, "Sonochemical Synthesis, Characterization, and Photocatalytic Activity of Perovskite ZnTiO3 Nanopowders," in *IEEE Transactions on Ultrasonics, Ferroelectrics, and Frequency Control*, vol. 63, no. 10, pp. 1663-1667, Oct. 2016. doi: 10.1109/TUFFC.2016.2593002.

[24] S. Zhang, Y. Zhu and J. Liu, "Multi-UAV Enabled Aerial-Ground Integrated Networks: A Stochastic Geometry Analysis," in *IEEE Transactions on Communications*, vol. 70, no. 10, pp. 7040-7054, Oct. 2022. doi: 10.1109/TCOMM.2022.3204662.

[25] Li-Peng Sun; Tiansheng Huang; Zihao Yuan; Mingjin Yang; Yan Huang; Peng Xiao; Bai-Ou Guan ., "Ultrasensitive Optofluidic Interferometer for Online Monitoring of Photocatalytic Reactions," in *Journal of Lightwave Technology*, vol. 37, no. 21, pp. 5435-5441, 1 Nov.1, 2019. doi: 10.1109/JLT.2019.2943872.

[26] R. Zhang, H. Wang, J. H. Park, H. -K. Lam and P. He, "Quasisynchronization of Reaction-Diffusion Neural Networks Under Deception Attacks," in *IEEE Transactions on Systems, Man, and Cybernetics: Systems*, vol. 52, no. 12, pp. 7833-7844, Dec. 2022. doi: 10.1109/TSMC.2022.3166554.

[27] M. H. Feda, Y. Khosravi, S. Darbari and B. Abdollahi Nejand, "Electrically Controlled Photocatalytic Reduction of Graphene Oxide Sheets by ZnO Nanostructures, Suitable for Tunable Optoelectronic Applications," in *IEEE Transactions on Electron Devices*, vol. 63, no. 8, pp. 3147-3153, Aug. 2016. doi: 10.1109/TED.2016.2582781.

[28] B. Bhuyan, M. Devi, A. Borah, B. Paul, S. S. Dhar and S. Vadivel, "Fabrication of a Novel ZnO/NiMoO4 Nanocomposite and Evaluation of Its Visible Light Driven Photocatalytic Performance," in *IEEE Transactions on Nanotechnology*, vol. 17, no. 4, pp. 743-750, July 2018. doi: 10.1109/TNANO.2018.2830811.

[29] Bakri Hossain Awaji; M. M. Kamruzzaman; Ahmad Althuniabt; Ibrahim Aqeel; Ibrahim Mohsen Khormi; Mani Gopalsamy ; Udayakumar Allimuthu. "Novel multiple access protocols against Q-learning-based tunnel monitoring using flying ad hoc networks". *Wireless Networks* vol 30, pp 987–1011 (2024). https://doi.org/10.1007/s11276-023-03534-y.

[30] V. M. Rosas-García, A. García-Pastrana and I. d. C. Sáenz-Tavera, "Theoretical Modeling of Photocatalytic Degradation Mechanism of Ethylene Over TiO2," in *IEEE Transactions on NanoBioscience*, vol. 21, no. 1, pp. 144-148, Jan. 2022. doi: 10.1109/TNB.2021.3102467.

[31] J. -S. Nam, K. C. Nam, K. -H. Choi, B. J. Park and J. -S. Jung, "Enhanced Photocatalytic Activity of Core-Shell ZnFe2O4@ZnO Nanoparticles for Visible Light Photodegradation," in *IEEE Transactions on Magnetics*, vol. 53, no. 11, pp. 1-5, Nov. 2017, Art no. 8300305. doi: 10.1109/TMAG.2017.2718034.

[32] R. Wang, M. A. Kishk and M. -S. Alouini, "Stochastic Geometry-Based Low Latency Routing in Massive LEO Satellite Networks," in *IEEE Transactions on Aerospace and Electronic Systems*, vol. 58, no. 5, pp. 3881-3894, Oct. 2022. doi: 10.1109/TAES.2022.3199682.

[33] Y. Ando, S. Tobe and H. Tahara, "Rapid Deposition of Photocatalytic Oxide Film by Liquid Feedstock Injection TPCVD in Open Air," in *IEEE Transactions on Plasma Science*, vol. 34, no. 4, pp. 1229-1234, Aug. 2006. doi: 10.1109/TPS.2006.878437.

[34] H. Ganie, I. U. Rahman, M. Sulaiman and K. Nonlaopon, "Solution of Nonlinear Reaction-Diffusion Model in Porous Catalysts Arising in Micro-Vessel and Soft Tissue Using a Metaheuristic," in *IEEE Access*, vol. 10, pp. 41813-41827, 2022. doi: 10.1109/ACCESS.2022.3168788.

[35] Manohar, C. Krishnamoorthi, K. C. B. Naidu and B. P. Narasaiah, "Dielectric, Magnetic Hyperthermia and Photocatalytic Properties of $Mg_{0.7}Zn_{0.3}Fe_2O_4$ Nanocrystals," in *IEEE Transactions on Magnetics*, vol. 56, no.

12, pp. 1-7, Dec. 2020, Art no. 5200207. doi: 10.1109/TMAG.2020.3024717.

[36] Natalia A. Trunina; Maxim E. Darvin; Krisztián Kordás; Anjana Sarkar; Jyri-Pekka Mikkola; Jürgen Lademann; Martina C. Meinke; Risto Myllylä; Valery V. Tuchin; Alexey P. Popov ., "Monitoring of TiO$_{\bf 2}$ and ZnO Nanoparticle Penetration Into Enamel and Dentine of Human Tooth IN VITRO and Assessment of Their Photocatalytic Ability," in *IEEE Journal of Selected Topics in Quantum Electronics*, vol. 20, no. 3, pp. 133-140, May-June 2014, Art no. 7300108. doi: 10.1109/JSTQE.2013.2276082.

[37] N. T. Eldabe, M. Y. Abou-zeid, A. S. A. Seliem, A. A. Elenna and N. Hegazy, "Thermal Diffusion and Diffusion Thermo Effects on Magnetohydrodynamics Transport of Non-Newtonian Nanofluid Through a Porous Media Between Two Wavy Co-Axial Tubes," in *IEEE Transactions on Plasma Science*, vol. 50, no. 5, pp. 1282-1290, May 2022. doi: 10.1109/TPS.2022.3161740.

[38] R. Wang, M. A. Kishk and M. -S. Alouini, "Evaluating the Accuracy of Stochastic Geometry Based Models for LEO Satellite Networks Analysis," in *IEEE Communications* Letters, vol. 26, no. 10, pp. 2440-2444, Oct. 2022. doi: 10.1109/LCOMM.2022.3194210.

[39] M. Tsujimoto, S. Moriguchi, S. Isoda, T. Kobayashi and T. Komatsu, "TEM analysis of Pt-particles embedded on TiO2 exhibiting high photocatalytic activity," in *Microscopy*, vol. 48, no. 4, pp. 361-366, Jan. 1999. doi: 10.1093/oxfordjournals.jmicro.a023689.

[40] W. Fu, "Optimization of Caching Update and Pricing Algorithm Based on Stochastic Geometry Theory in Video Service," in *IEEE Access*, vol. 10, pp. 85470-85482, 2022. doi: 10.1109/ACCESS.2022.3198667.

[41] X. Feng and H. Huang, "A fuzzy-set-based Reconstructed Phase Space method for identification of temporal patterns in complex time series," in *IEEE Transactions on Knowledge and Data Engineering*, vol. 17, no. 5, pp. 601-613, May 2005, doi: 10.1109/TKDE.2005.68.

[42] K. Yoshida, T. Nozaki, T. Hirayama and N. Tanaka, "In situ High-Resolution Transmission Electron Microscopy of Photocatalytic Reactions by Excited Electrons in Ionic Liquid," in *Microscopy*, vol. 56, no. 5, pp. 177-180, Oct. 2007. doi: 10.1093/jmicro/dfm021.

[43] N. Biasi, P. Seghetti, M. Mercati and A. Tognetti, "A Reaction-Diffusion Heart Model for the Closed-Loop Evaluation of Heart-Pacemaker Interaction," in *IEEE Access*, vol. 10, pp. 121249-121260, 2022. doi: 10.1109/ACCESS.2022.3222830.

[44] Y. Ando, S. Y. Chen and Y. Noda, "Photocatalytic Titanium Oxide Film Deposition by Atmospheric TPCVD Using Air as the Working Gas," in *IEEE Transactions on Plasma Science*, vol. 41, no. 8, pp. 1850-1855, Aug. 2013. doi: 10.1109/TPS.2013.2247066.

[45] Shifeng Fang; Lida Xu; Huan Pei; Yongqiang Liu; Zhihui Liu; Yunqiang Zhu; Jianwu Yan; Huifang Zhang., "An Integrated Approach to Snowmelt Flood Forecasting in Water Resource Management," in *IEEE Transactions on Industrial Informatics*, vol. 10, no. 1, pp. 548-558, Feb. 2014. doi: 10.1109/TII.2013.2257807.

[46] R. Dhanalakshmi, P. Reddy Vanga, M. Ashok and N. V. Giridharan, "The Effect of a 0.5 T Magnetic Field on the Photocatalytic Activity of Recyclable Nd-modified BiFeO 3 Magnetic Catalysts," in *IEEE Magnetics Letters*, vol. 7, pp. 1-4, 2016, Art no. 2106904. doi: 10.1109/LMAG.2016.2610406.

[47] Stasinopoulos, N., Chalaris, M., Tezari, A., & Kravari, K. (2023). The Endless Possibilities of Modelling of Toxic Chemical Warfare Agents and Possible Impacts of Their Release in Water Sensitive Areas. *WSEAS Transactions on Environment and Development*, vol 19, 998-1007. doi: 10.37394/232015.2023.19.94.

[48] Öztekin, R., & SPONZA, D. (2023). The Removal of Pollutants by Sonication using Nitrogen Gas in Textile Industry Wastewater: Comparison of Energy Consumption and Cost Analysis with Other Advanced Oxidation Processes. *WSEAS Transactions on Environment and Development*, vol 19. Pp 45-69, https://doi.org/10.37394/232015.2023.19.5.

APPENDIX

Table 1. High rate $\ln\frac{A_o}{A_T}$constant analysis for visible light irradiation photoactivity

Irradiation Time (m)	$\ln\frac{A_o}{A_T}$									
	RhB					4-CP				
	g-C_3N_4	$MnWO_4$	GMW_1	GMW_2	GMW_3	g-C_3N_4	$MnWO_4$	GMW_1	GMW_2	GMW_3
0	0.12	0.17	0.20	0.18	0.08	0.13	0.15	0.13	0.07	0.05
20	0.36	0.28	0.26	0.140	0.12	0.2	0.45	0.21	0.13	0.093
40	0.55	0.32	0.274	0.192	0.15	0.9	0.62	0.28	0.162	0.132
60	0.74	0.48	0.32	0.25	0.17	0.34	0.69	0.39	0.245	0.152
80	0.93	0.69	0.41	0.32	0.19	0.24	0.70	0.43	0.29	0.171
100	1.22	0.763	0.50	0.39	0.23	0.14	0.77	0.48	0.34	0.19

Table 2. Chemical oxygen demand Removal Efficiency(%)of RhB and 4-CP dyes

Irradiation Time (m)	Chemical oxygen demand Removal Efficiency(%)									
	RhB					4-CP				
	g-C_3N_4	$MnWO_4$	GMW_1	GMW_2	GMW_3	g-C_3N_4	$MnWO_4$	GMW_1	GMW_2	GMW_3
0	31	35	36	35	36	43	28	48	39	34
20	35	39	68	55	63	51	34	53	36	55
40	38	35	72	49	69	56	48	62	42	66
60	43	40	75	54	74	59	52	70	56	78
80	47	44	70	62	82	50	57	73	65	82
100	45	38	74	69	92	46	56	76	75	86

Table 4. The high rate constant for photocatalysts under visible light

Irradiation Time in minutes	$\ln\frac{K_t}{K_0}$									
	RhB					4-CP				
	g-C_3N_4	$BiVO_4$	GBV_1	GBV_2	GBV_3	g-C_3N_4	$BiVO_4$	GBV_1	GBV_2	GBV_3
0	0.11	0.17	0.15	0.13	0.17	0.12	0.15	0.12	0.18	0.14
20	0.16	0.25	0.32	0.45	0.52	0.161	0.242	0.26	0.42	0.52
40	0.19	0.34	0.52	0.92	1.04	0.22	0.43	0.44	0.73	0.86
60	0.23	0.45	0.68	1.25	1.23	0.26	0.63	0.62	1.13	1.45
80	0.27	0.53	0.85	1.4	1.42	0.34	0.72	0.84	1.36	1.92
100	0.32	0.60	0.94	1.54	1.81	0.43	0.87	0.92	1.59	2.26

Table 5. Chemical Oxygen Demand, Removal Efficiency dyes, using g-C_3N_4/$BiVO_4$ photocatalyst

Irradiation Time in minutes	**Chemical Oxygen Demand Removal Efficiency**									
	RhB					**4-CP**				
	g-C_3N_4	**$BiVO_4$**	**GBV_1**	**GBV_2**	**GBV_3**	**g-C_3N_4**	**$BiVO_4$**	**GBV_1**	**GBV_2**	**GBV_3**
0	31	29	24	32	33	25	28	22	26	30
20	56	34	37	40	42	30	35	34	35	42
40	61	48	41	46	57	33	42	38	39	54
60	67	52	54	52	69	37	46	42	43	62
80	65	60	57	56	76	44	50	47	49	69
100	62	65	63	60	86	47	56	52	54	72

Table 7. The relationship between g-C_3N_4/$ZnWO_4$ of $\ln\frac{Cons_o}{Cons_T}$ (%) under visible light irradiation time.

Irradiation Time in minutes	**$\ln\frac{Cons_o}{Cons_T}$ (%)**									
	RhB					**4-CP**				
	g-C_3N_4	**$ZnWO_4$**	**GZW_1**	**GZW_2**	**GZW_3**	**g-C_3N_4**	**$ZnWO_4$**	**GZW_1**	**GZW_2**	**GZW_3**
0	0.085	0.17	0.15	0.13	0.10	0.09	0.05	0.17	0.12	0.14
20	0.12	0.20	0.24	0.25	0.32	0.11	0.109	0.24	0.20	0.27
40	0.14	0.24	0.29	0.42	0.54	0.14	0.12	0.37	0.31	0.41
60	0.15	0.28	0.38	0.65	0.73	0.16	0.14	0.41	0.43	0.64
80	0.19	0.31	0.45	0.74	1.02	0.19	0.19	0.472	0.50	0.92
100	0.21	0.37	0.52	0.84	1.21	0.21	0.24	0.54	0.61	1.18

Table 8. The Chemical Oxygen Demand Removal Efficiency of g-C_3N_4/$ZnWO_4$.

Irradiation Time in minutes	**Chemical Oxygen Demand Removal Efficiency (%)**									
	RhB					**4-CP**				
	g-C_3N_4	**$ZnWO_4$**	**GZW_1**	**GZW_2**	**GZW_3**	**g-C_3N_4**	**$ZnWO_4$**	**GZW_1**	**GZW_2**	**GZW_3**
0	21	24	29	24	25	22	21	20	23	25
20	30	36	35	37	41	36	30	33	35	34
40	38	46	46	48	61	48	42	45	42	46
60	43	63	58	52	70	45	55	52	55	56
80	48	72	63	64	83	51	67	57	59	67
100	52	80	72	78	97	55	78	62	63	85

Table 10. The kinetic plot relating to the degradation rate at different photocatalysts

Irradiation Time in minutes	$\ln C_0/C$									
	RhB					4-CP				
	g-C_3N_4	$CuWO_4$	$GCuW_1$	$GCuW_2$	$GCuW_3$	g-C_3N_4	$CuWO_4$	$GCuW_1$	$GCuW_2$	$GCuW_3$
0	1.05	1.03	1.029	1.08	1.02	1.072	1.09	1.074	1.096	1.01
20	0.97	0.90	0.92	0.84	0.79	0.97	0.96	0.85	0.87	0.85
40	0.93	0.84	0.83	0.78	0.52	0.92	0.92	0.76	0.72	0.62
60	0.90	0.78	0.63	0.68	0.44	0.89	0.86	0.58	0.58	0.54
80	0.87	0.72	0.56	0.57	0.38	0.83	0.75	0.49	0.42	0.30
100	0.84	0.70	0.46	0.50	0.30	0.76	0.66	0.35	0.25	0.12

Table 11. Chemical Oxygen Demand removal efficiency of various photocatalysts over 0-100 minutes.

Irradiation Time in minutes	Chemical Oxygen Demand Removal Efficiency(%)									
	RhB					4-CP				
	g-C_3N_4	$CuWO_4$	$GCuW_1$	$GCuW_2$	$GCuW_3$	g-C_3N_4	$CuWO_4$	$GCuW_1$	$GCuW_2$	$GCuW_3$
0	22	42	55	44	61	26	56	29	32	30
20	35	49	64	52	63	32	48	32	40	38
40	41	52	63	68	67	35	42	42	44	47
60	45	53	65	73	72	38	52	55	53	56
80	53	57	63	75	75	42	56	58	59	63
100	59	65	74	79	80	46	60	62	64	70

Table 13. Comparison analysis of nanocomposites over measures of degradation rate constant K(m^{-1}), COD removal efficiency, and Degradation rate.

Parameters		**Samples**			
		$g\text{-}C_3N_4$/ $MnWO_4$	$g\text{-}C_3N_4$/ $BiVO_4$	$g\text{-}C_3N_4$/ $ZnWO_4$	$g\text{-}C_3N_4$/ $CuWO_4$
degradation rate constant K(m^{-1})	RhB	0.0842	0.0821	0.0914	0.0812
	4-CP	0.0504	0.0643	0.0731	0.0715
COD removal Efficiency (%)	RhB	92	86	97	80
	4-CP	86	72	85	70
Degradation rate at 100 min	RhB	97	89	99	89
	4-CP	92	94	89	75

Contribution of Individual Authors to the Creation of a Scientific Article (Ghostwriting Policy)

The authors equally contributed in the present research, at all stages from the formulation of the problem to the final findings and solution.

Sources of Funding for Research Presented in a Scientific Article or Scientific Article Itself

No funding was received for conducting this study.

Conflict of Interest

The authors have no conflicts of interest to declare that are relevant to the content of this article.